Earthquake Engineering, Tenth World Conference © 1992 Balkema, Rotterdam. ISBN 90 5410 060 5

Seismic analysis of rectangular tunnels in soft ground

Joseph Penzien
International Civil Engineering Consultants, Inc., Berkeley, Calif., USA

C. H. Chen & Y. J. Lee
National Taiwan University, Taipei, Taiwan

W. Y. Jean
D&E Services Company, Taipei, Taiwan

ABSTRACT: Practical analytical procedures are presented for assessing the seismic performance of rectangular concrete-lined tunnels located in soft soils as follows: (1) generating free-field ground motions in a horizontally-layered soil medium, (2) calculating cross-sectional deformations and overall global response of the lining to the free-field motions, including soil-structure interaction effects, and (3) evaluating separations in the lining's transverse joints. Numerical results are given to show the general nature of seismic performance for selected tunnel linings.

1 INTRODUCTION

To provide for the flow of automobile and train traffic in metropolitan areas, rectangular underground tunnels having reinforced concrete linings are commonly constructed by the cut-and-cover method. Often, these tunnels are located in soft ground which can experience high intensity motions due to the occurrence of large earthquakes. It has been common practice to design the linings on the basis that they will deform in a manner totally compatible with the free-field ground displacements (Kuesel 1969; DORTS 1988); even though, methods of analysis have been suggested which consider the effects of soil-structure interaction (Aoki, Y. 1973; Okamoto, S. and Tamura, C. 1973; Penzien, J. and Tseng, W. S. 1981). The purpose of this paper is to advance some of the more practical procedures for (1) predicting possible free-field ground displacements along the tunnel alignment which are critical to the lining response, (2) evaluating lining deformations produced by these displacements, including soil-structure interaction effects, and (3) estimating separations of transverse joints in the lining, and to present numerical results generated for the Sungshan Railway Extension project in Taipei, Taiwan, R.O.C..

2 FREE-FIELD GROUND MOTIONS

As is common practice, one set of horizontal free-field ground motions can be developed assuming vertically propagating shear waves in a horizontally-layered soil medium with the surface motions used for control purposes (Seed, H. B. and Idriss, I. M. 1970; Schnabel, P. B., et al. 1972). These control motions, which are usually specified to be compatible with a design response spectrum, can be obtained by systematically adjusting field-recorded or synthetically-generated accelerograms.

Assuming upward travelling incident shear-waves in the uniform half-space below the layered medium, which can be represented as a series of harmonics, one can calculate the corresponding upward and downward travelling harmonics in each layer, and the corresponding downward travelling harmonics in the half-space resulting from their interactions with the layered system. Decomposing the specified free-field surface acceleration time-history into its harmonics and satisfying the surface zero stress condition and the displacement and stress compatibility conditions at each interface of the layered system, one can calculate the amplitude and phase angle of each upward travelling harmonic and each downward travelling harmonic in each layer and in the half-space, thus providing time-histories of ground acceleration and displacement at all elevation levels in the layered media which are compatible with the soil modelling and the specified free-field surface motions. In carrying out these calculations, it is necessary to reduce the small-strain ($\gamma = 10^{-6}$) shear-modulus values and increase the corresponding damping ratios representing the soil in each layer in accordance with the standard equivalent linearization procedure and the appropriate shear-modulus and damping-ratio relations $G(\gamma)/G(\gamma = 10^{-6})$ and $\xi(\gamma)$ expressed as functions of shear strain (γ). For the seismic response calculations referred herein, the effective shear strain at each elevation was taken as 65% of the corresponding maximum strain. In the equivalent linearization procedure, iteration must be used in finalizing the strain-compatible shear-modulus

and damping-ratio values.

Having obtained the horizontal free-field ground displacement time-histories at discrete elevations over the height of the lining cross-section by the above procedure, the shear (or racking) deformation of the cross-section can be evaluated by the finite-element procedure described subsequently, which includes the effects of soil-structure interaction.

To calculate overall global response of the lining, i.e., its combined axial and bending deformation, components of free-field ground displacement in a vertical plane at positions along the tunnel's longitudinal axis, under the most critical ground motion condition possible, are required. In calculating these displacement time-histories, use is made of the horizontal free-field ground displacement time history $V(t)$ at the mid-height position of the tunnel cross-section as generated by the above-described vertically-propagating shear-wave model.

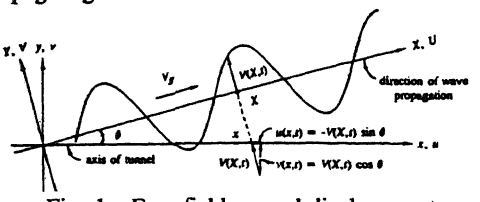

Fig. 1 Free-field ground displacements for global analysis

However, in this application, it is assumed that displacement $V(t)$ is produced by a single train of shear waves travelling at velocity V_{ff} at an angle θ from the longitudinal axis of the tunnel as shown in Fig. 1; thus, the free-field soil displacements along the X-axis, but normal to it, are given by

$$V(X,t) = \sum_n V(i\bar{\omega}_n)\exp[i\bar{\omega}_n(t - \frac{X}{V_{ff}})] \qquad (1)$$

in which $V(i\bar{\omega}_n)$ are the complex amplitudes of the discrete harmonics contained in $V(t)$ as generated by the FFT (Fast Fourier Transform) algorithm. The corresponding components of displacement along the x-axis in the x- and y-directions are

$$u(x,t) = -\sin\theta \sum_n V(i\bar{\omega}_n)\exp[i\bar{\omega}_n(t - \frac{x\cos\theta}{V_{ff}})]$$
$$v(x,t) = \cos\theta \sum_n V(i\bar{\omega}_n)\exp[i\bar{\omega}_n(t - \frac{x\cos\theta}{V_{ff}})] \qquad (2)$$

These free-field ground displacements are used subsequently to evaluate overall global response of the lining, including soil-structure interaction effects.

3 CROSS-SECTION RACKING ANALYSIS

The most severe free-field ground motion environment causing the lining cross-section to undergo racking (shear-type) deformation is that condition produced by the vertically travelling shear waves in the layered medium. The most critical time when maximum racking occurs can be taken as that instant when the relative horizontal free-field soil displacement between the top and bottom positions of the lining cross-section is a maximum. At this instant, the horizontal free-field ground displacement profile over the entire depth of the lining is known.

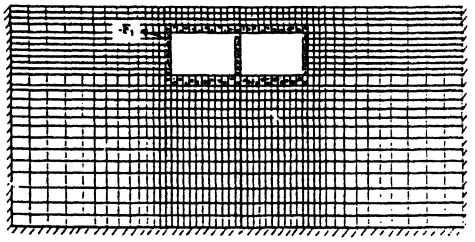

Fig. 2 Finite-element modelling of soil and lining

Since the lining interacts with the surrounding soil in essentially a quasi-static fashion, the racking analysis can be carried out in three steps using finite-element modelling of the lining and soil as shown in Fig. 2 and static loadings. Step 1--Using the finite element model of the lining cross-section only, static forces (represented by vector $\mathbf{F}_1$) are calculated, which, when applied to its outer-boundary nodes, will deform the cross-section so that these nodes displace exactly the same as do the corresponding points in the free-field soil (no lining present). The stresses in the cross-section under this deformed shape are calculated by the standard finite-element procedure. Step 2--The free-field shear stress distribution acting on the outer boundary of the rectangular soil element to be displaced by the cross-section is discretized, giving static forces (represented by vector $\mathbf{F}_2$) acting in the same nodal coordinates as those of the outer-boundary of the cross-section. If this soil element is now replaced by the lining cross-section and full bond is assumed at its outer-boundary with the soil, the external static forces (represented by vector $\mathbf{F}_3$) required in the coordinates of the cross-section outer-boundary nodes to cause these same nodes of the combined soil/lining model to displace in a manner totally compatible with the corresponding free-field soil displacements are the components in vector $\mathbf{F}_3$ as defined by $\mathbf{F}_3 \equiv \mathbf{F}_1 - \mathbf{F}_2$. Step 3--Since the external static forces contained in $\mathbf{F}_3$ do not actually exist, they must be canceled out by applying them in opposite directions to the combined soil/lining model as shown in Fig. 2. The resulting stresses in the lining must be superimposed on the corresponding stresses generated in Step 1 to obtain the desired critical racking stresses in the lining.

4 GLOBAL RESPONSE ANALYSIS

The horizontal and vertical free-field soil displacements along the longitudinal axis position of the tunnel as expressed by Eqs. (2) will be used to evaluated the overall global response of the lining. Because the mass of the lining is much less than the mass of the soil it displaces, the global response of the lining can be carried out in a quasi-static fashion using the corresponding equations which govern its axial and bending deformation, namely

$$\begin{aligned} \frac{\partial^2 u_l(x,t)}{\partial x^2} - \frac{k_x}{AE} u_l(x,t) &= -\frac{k_x}{AE} u(x,t) \\ \frac{\partial^4 v_l(x,t)}{\partial x^4} + \frac{k_y}{EI} v_l(x,t) &= +\frac{k_y}{EI} v(x,t) \end{aligned} \tag{3}$$

in which $u(x, t)$ and $v(x, t)$ are the free-field ground displacements given by Eqs. (2), u_l and v_l are the lining displacements along its centrordal axis, k_x and k_y are subgrade moduli in the x- and y-directions, and AE and EI are the axial and flexural stiffnesses of the lining.

Substituting Eqs. (2) into Eqs. (3) and obtaining the steady state solutions gives

$$\begin{aligned} u_l(x,t) &= -\sin\theta \sum_n \frac{V(i\bar{\omega}_n)}{(1+\phi_{un})} \exp[i\bar{\omega}_n(t - \frac{x\cos\theta}{V_{ff}})] \\ v_l(x,t) &= \cos\theta \sum_n \frac{V(i\bar{\omega}_n)}{(1+\phi_{vn})} \exp[i\bar{\omega}_n(t - \frac{x\cos\theta}{V_{ff}})] \end{aligned} \tag{4}$$

in which

$$\phi_{un} \equiv \frac{AE\bar{\omega}_n^2\cos^2\theta}{k_x V_{ff}^2} \quad ; \quad \phi_{vn} \equiv \frac{EI\bar{\omega}_n^4\cos^4\theta}{k_y V_{ff}^4} \tag{5}$$

Note that when ϕ_{un} and ϕ_{vn} equal zero which corresponds to k_x and k_y being equal to infinity, the tunnel displacements given by Eq. (4) are identical to the free-field soil displacements given by Eqs. (2), i.e., no soil-structure interaction effects are present.

The axial and bending normal strains in the lining at coordinate position y of the cross-section can be obtained by substituting Eqs. (4) into the relations

$$\epsilon_a(x,t) = \frac{\partial u_l(x,t)}{\partial x} \quad ; \quad \epsilon_b = -y\frac{\partial^2 v_l(x,t)}{\partial x^2} \tag{6}$$

giving

$$\begin{aligned} \epsilon_a(x,t) &= +\frac{\sin\theta\cos\theta}{V_{ff}} i\sum_n \frac{\bar{\omega}_n V(i\bar{\omega}_n)}{(1+\phi_{un})} \exp[i\bar{\omega}_n(t - \frac{x\cos\theta}{V_{ff}})] \\ \epsilon_b(x,t) &= +y\frac{\cos^3\theta}{V_{ff}^2} \sum_n \frac{\bar{\omega}_n^2 V(i\bar{\omega}_n)}{(1+\phi_{vn})} \exp[i\bar{\omega}_n(t - \frac{x\cos\theta}{V_{ff}})] \end{aligned} \tag{7}$$

The combined normal strain $\epsilon(x, t)$ at position y is now obtained by summing Eqs. (7), i.e., using

$$\epsilon(x,t) = \epsilon_a(x,t) + \epsilon_b(x,t) \tag{8}$$

Upon examining numerical results given by Eqs. (7) for the maximum value of $|y|$ on a cross-section and for the critical value of θ, which is close to 45°, one finds that $|\epsilon_a(x,t)|_{max}$ is much greater than $|\epsilon_b(x,t)|_{max}$. Further, since each harmonic in $\epsilon_a(x,t)$ is 90° out-of-phase with the corresponding harmonic in $\epsilon_b(x,t)$, $|\epsilon_a(x,t)|_{max}$ will occur at an instant of time quite different from that at which $|\epsilon_b(x,t)|_{max}$ occurs; thus, the square-root-of-the-sum-of-squares (SRSS) method could be used to estimate $|\epsilon(x,t)|_{max}$, i.e.,

$$|\epsilon(x,t)|_{max} = [|\epsilon_a(x,t)|_{max}^2 + |\epsilon_b(x,t)|_{max}^2]^{\frac{1}{2}} \tag{9}$$

In view of the above observations, the bending contribution to $|\epsilon(x,t)|_{max}$ is negligible for the critical value of θ which is very close to 45°. Therefore, one can estimate the critical value of normal strain using the first of Eqs. (7) alone with θ set equal to 45°, i.e., using

$$|\epsilon(x,t)|_{max} \doteq \frac{1}{2V_{ff}} |\sum_n i\frac{\bar{\omega}_n V(i\bar{\omega}_n)}{(1+\phi_{un})} \exp[i\bar{\omega}_n(t - \frac{x}{\sqrt{2}\,V_{ff}})]|_{max} \tag{10}$$

in which $\phi_{un} = AE\bar{\omega}_n^2/2k_x V_{ff}^2$. The subgrade modulus k_x cannot be evaluated rigorously for a given soil/liner system; however, for practical solutions, it can be approximated using $k_x \doteq 3G = 3\rho V_{si}^2$ in which ρ is the mass density of the soil adjacent to the lining, G is its effective shear modulus in the dominate region controlling soil-structure interaction, and V_{si} is the corresponding shear wave velocity. Note that V_{ff}, as defined earlier, is that shear wave velocity controlling the train of free-field travelling waves approaching the tunnel alignment; while V_{si} is the effective shear wave velocity controlling soil/structure interaction. These two shear-wave velocities may be significantly different from each other. Obviously, considerable judgement must be used in assigning their numerical values, after taking into consideration known factors such as geometry of soil layers relative to tunnel location, results of soil tests, and levels of soil shear strain produced by the free-field motions and by the soil-lining interaction. In considering the latter factor, one should note that the shear strains produced by the free-field ground motions and by soil-structure interaction, at the outer-boundary location of the lining cross-section, are given, respectively, by

$$\gamma_{ff}(X,t) = \frac{\partial V(X,t)}{\partial X} \quad ; \quad \gamma_{si}(x,t) = \frac{AE}{\rho\rho V_{si}^2}\frac{\partial \epsilon_a(x,t)}{\partial x} \tag{11}$$

in which p is the outside perimeter dimension of the cross-section. Making use of $X = x\cos\theta$, $\theta = 45°$, Eq. (1), and the first of Eqs. (7), these shear-strain relations become

$$\gamma_{ff}(x,t) = -\frac{i}{V_{ff}}\sum_n \bar{\omega}_n V(i\bar{\omega}_n)\exp[i\bar{\omega}_n(t - \frac{x}{\sqrt{2}V_{ff}})]$$
$$\gamma_{sf}(x,t) = \frac{AE}{2\sqrt{2}p\rho V_{sf}^2 V_{ff}^2}\sum_n \frac{\bar{\omega}_n^2 V(i\bar{\omega}_n)}{(1+\phi_{sf})}\exp[i\bar{\omega}_n(t - \frac{x}{\sqrt{2}V_{ff}})] \quad (12)$$

5 SEPARATION OF TRANSVERSE JOINTS

The axial strains described in the previous section were evaluated assuming no transverse joints to be present in the tunnel lining. Placement of such joints in the lining would reduce these strains to zero at the joints and would also reduce them at intermediate locations between adjacent pairs of joints. Using the first of Eqs. (3) and assuming the dominant free-field soil wave lengths producing $|\epsilon(x,t)|_{max}$ are long compared with the joint interval distance L, it can be shown that the ratio of the maximum absolute strain at the midway-point ($x = 0$) between an adjacent pair of joints to the maximum absolute strain given by Eq. (10) is

$$|\epsilon(0,t)|_{max}/|\epsilon(x,t)|_{max} = [1 - \frac{2}{\exp(\beta L/2) + \exp(-\beta L/2)}] \quad (13)$$

in which $\beta \equiv \sqrt{k_x/AE}$. Further, it can be shown that the strain reductions in a segment of lining tributary to a particular joint will allow it to separate a distance Δ_j as expressed by

$$\frac{\Delta_j}{L|\epsilon(x,t)|_{max}} = \frac{2}{\beta L}\left[\frac{\exp(\beta L/2) - \exp(-\beta L/2)}{\exp\beta L/2) + \exp(-\beta L/2)}\right] \quad (14)$$

6 CASE STUDY

A case study is presented to demonstrate use of the above analytical procedures and to show the general nature of seismic response for selected tunnel linings.

6.1 Lining cross-sections

The basic lining cross-section used in this case study is shown in Fig. 3. In this exact form, it is representative of one type of cross-section designed for the Sungshan Railway Extension. Variations on the wall and slab thicknesses, but not on the outside dimensions, of this cross-section were introduced to investigate the influence of tunnel stiffness on global response. The Young's modulus E and Poisson's ratio ν used for the concrete of the lining were 22,800 MN/m^2 and 0.20, respectively. The top of the cross-section is located approximately 3 meters under the ground surface.

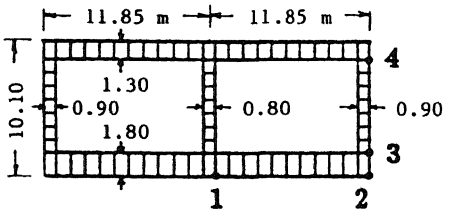

Fig. 3 Basic lining cross-section

6.2 Soil properties

The soil profile used for this case study consists of 19 layers of clay and sand materials resting on the half-space below. The total depth of the layered system is 48 m. The soil properties are quite variable over the entire depth consistent with the soft site-condition of the Taipei basin.

6.3 Free-field ground motions

The control free-field ground acceleration time-history representing surface motion was first generated to be compatible with the normalized pseudo-acceleration response spectrum for 5 percent damping as given by

$$\begin{aligned} S_a &= 1g & T &\le 0.054\,\text{sec} \\ S_a &= (0.238 + 14.11T)g & 0.054 &\le T \le 0.20\,\text{sec} \\ S_a &= 3.06g & 0.20 &\le T \le 0.168\,\text{sec} \\ S_a &= 8.661g/T^2 & T &\ge 1.68\,\text{sec} \end{aligned} \quad (15)$$

which represents the Taipei basin site conditions (DORTS 1988). Then it was scaled to a PGA (peak ground acceleration) level equal to 0.18 g giving the resulting accelerogram shown in Fig. 4.

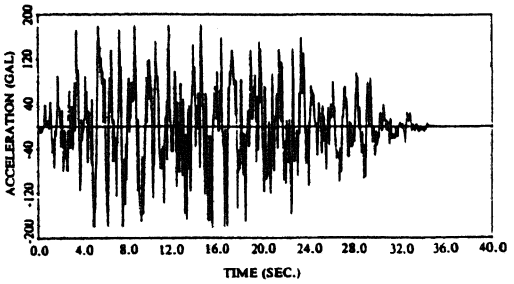

Fig. 4 Free-field surface accelerogram

Using this control motion and the vertically-travelling shear-wave model of the 19-layer soil system, the time-histories of horizontal ground displacement at discrete

values of elevation from top to bottom of the lining cross-section were obtained.

6.4 Racking analysis results

A racking analysis as described in Sec. 3 was carried out for the lining cross-section shown in Fig. 3 using the 19-layer soil system described above and the control acceleration time-history shown in Fig. 4. The critical free-field soil displacement profile obtained in this analysis is shown in Fig. 5. Dividing the difference between the soil displacements at the top and bottom cross-section locations in this profile by the depth of the cross-section, one obtains an average free-field soil strain over this depth equal to 11.0×10^{-4} radians, which will be designated subsequently by γ_s.

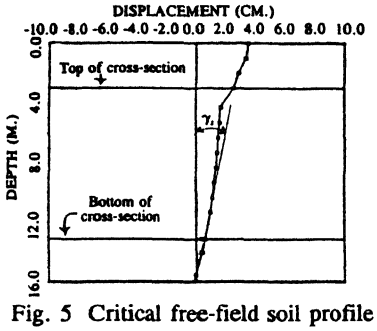

Fig. 5 Critical free-field soil profile

Completing Steps 1, 2, and 3 as described in Sec. 3 and using superposition, the combined critical racking stresses in the cross-section and the corresponding nodal displacements were obtained. From the nodal displacements, a racking angle for the lining cross-section was obtained which is defined herein as the angle change between the straight line connecting Nodes 1 and 2 and the straight line connecting Nodes 3 and 4; see Fig. 3. The numerical value of this angle change (γ_t) was found to be 4.6×10^{-4} radians. Dividing this angle by the critical free-field soil racking angle, one obtains $\gamma_t/\gamma_s = 4.6/11.0 = 0.42$ showing that for this basic cross-section, soil-structure interaction effects greatly reduce the racking deformations.

To study the importance of soil-structure interaction effects on the racking deformations of cross-sections when the relative stiffnesses of lining and surrounding soils are changed, parametric studies were carried out using (1) the same critical free-field soil displacement profile shown in Fig. 5, (2) the same 19-layer geometry in the soil-structure interaction analysis but with all soil shear moduli (G) changed by a factor α from those values (G_0) used in the above case study ($\alpha \equiv G/G_0$), (3) the same outside geometry of cross-section as shown in Fig. 3 but with all wall and slab thicknesses (t) increased by a factor β from those values (t_0) shown in the figure ($\beta \equiv t/t_0$) and (4) the same concrete Young's modulus (E) and Poisson's ratio given previously. The results of these parametric studies are shown in Figs. 6 and 7.

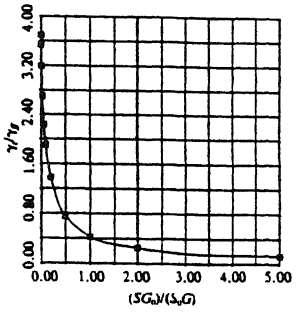

Fig. 6 Racking angle ratio vs. lining/soil stiffness ratio

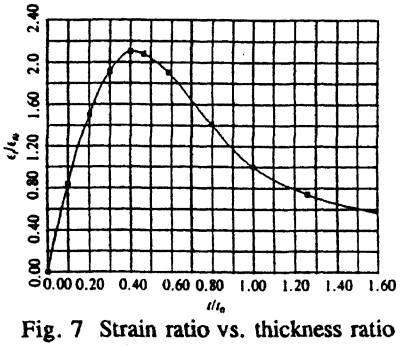

Fig. 7 Strain ratio vs. thickness ratio

Figure 6 shows the ratio of cross-section racking angle to the free-field soil racking angle (γ_t/γ_s) plotted as the ordinate with the ratio $(SG_0)/(S_0G)$ plotted as the abscissa, in which S_0 represents the racking stiffness of the basic cross-section shown in Fig. 3 and S is the corresponding variable stiffness. As seen in this figure, when $S = S_0$ and $G = G_0$, i.e., $(SG_0)/(S_0G) = 1$, $(\gamma_t/\gamma_s) = 0.42$ as stated above. When $(SG_0)/(S_0G)$ reduces towards zero, the ratio (γ_t/γ_s) increases to the value 3.64 corresponding to $\gamma_t = (3.64)(11.0)(10^{-4}) = 40 \times 10^{-4}$ radians. Note that this angle corresponds to the racking angle of a rectangular tunnel having no lining which is greater than the racking angle of the free-field soil having no tunnel by the factor 3.64. As $(SG_0)/(S_0G)$ increases from zero, the ratio (γ_t/γ_s) continues to decrease showing a corresponding increase in soil-structure interaction effects.

Letting $G = G_0$ so that the ratio $(SG_0)/(S_0G)$ reduces to the cross-section stiffness ratio (S/S_0), the graph of Fig. 6 can be converted to that shown in Fig. 7, where ϵ_0 refers to the critical flexure strain in the basic cross-section of Fig. 3 due to racking and ϵ refers to the corresponding critical strain in the modified cross-section due to changing all wall, roof, and floor slab thicknesses from their basic values (t_0) to their varied

values (t). This conversion is accomplished by recognizing that

$$(S/S_0) \doteq (t/t_0)^3 \tag{16}$$

and

$$(\gamma_t/\gamma_s) = (\gamma_{t0}/\gamma_s)(\gamma/\gamma_{t0}) \doteq (\gamma_{t0}/\gamma_s)(\epsilon/\epsilon_0)(t_0/t) \tag{17}$$

in which γ_{t0} is the racking angle of the basic cross-section in Fig. 3 equal to 4.6×10^{-4} radians, γ_t is the corresponding racking angle of the modified cross-section, and γ_s is the critical free-field racking angle equal to 11×10^{-4} radians. Using these equations, the graph of Fig. 7 is obtained directly from the graph of Fig. 6. Note that as the thickness ratio reduces from the basic value $t/t_0 = 1$, the flexure strain ratio ϵ/ϵ_0 increases. Two partially offsetting effects are taking place. If the cross-section's racking-angle was held constant, the strain ratio would decrease with decreasing values of t/t_0 and, if the thickness ratio was held constant, the strain ratio would increase with increasing racking angles. The latter effect is dominant in this case. However, below the value $t/t_0 = 0.4$, decreasing values of t/t_0 result in decreasing values of ϵ/ϵ_0; thus, showing the former effect is dominating. Certainly, as the ratio t/t_0 goes to zero, the tunnel has no stiffness whatsoever so the racking angle is the same as the racking angle of the rectangular tunnel having no lining. While this particular racking angle is large, the strain goes to zero because the thicknesses t goes to zero. As the thickness ratio increases beyond the basic value $t/t_0 = 1$, the ratio ϵ/ϵ_0 continues to reduce due to soil-structure interaction effects.

6.5 Global response results

Maximum axial strains were calculated by Eq. (10) for the cross-section shown in Fig. 3 using the 19-layer soil medium described earlier, along with its associated soil properties, and the surface control motion presented in Fig. 4. Unfortunately, limited space does not permit a detailed presentation of the results herein. Let it suffice to simply report the most critical result, namely the maximum normal stress on the cross-section which was evaluated to be approximately one-third the concrete compressive strength, i.e.,

$$|\sigma(x,t)|_{max} = E\,|\epsilon(x,t)|_{max} \doteq \frac{1}{3}f_c' \tag{18}$$

Considering that the free-field soil motion was assumed to be a single wave train moving at the most critical angle $\theta = 45°$, which is an extremely conservative assumption, the maximum stress calculated by Eq. (18) can be reduced substantially in estimating a more realistic value. Obviously, considerable judgement is required in making this final assessment.

6.6 Effects of transverse joints

Once the joint spacing L and the factor $\beta \equiv \sqrt{k_x/AE}$ are known, Eqs. (13) and (14) can be used to obtain the mid-point axial strain and the corresponding joint separation. Since the maximum strain $|\epsilon(x,t)|_{max}$ is usually relatively low, placement of transverse joints for the purpose of reducing seismically induced strains is unnecessary. Should they be present for other reasons, their separations as caused by seismic effects can be tolerated using appropriate joint seals.

7 CONCLUDING STATEMENT

In assessing the seismic performance of tunnel linings, it is necessary to include soil-structure interaction effects. Once this is done, the deformations produced will usually be within tolerable limits.

8 ACKNOWLEDGEMENT

The numerical results of the CASE STUDY were generated by the authors under a contract by and between Eastern International Engineers, Inc. and China Engineering Consultants, Inc.

REFERENCES

Aoki, Y. 1973. Seismic design spectra for trench type tunnel. Proc. Japan Society of Civil Eng., No. 211.

Department of Rapid Transit Systems (DORTS) 1988. Civil engineering design manual. Taipei Municipal Government, R.O.C.

Kuesel, T. R. 1969. Earthquake design criteria for subways. Proc. ASCE. 95, ST6, 1213-1231.

Okamoto, S. and C. Tamura 1973. Behavior of subaqueous tunnels during earthquakes. Earthquake Engineering and Structural Dynamics. 1: 253-166.

Penzien, J. and W. S. Tseng 1981. Seismic analysis of subaqueous tunnels. Workshop on Earthquake Engineering, The Chinese Institute of Civil and Hydraulic Engineering, Taipei.

Schnabel, P. B., et al. 1972. SHAKE - A computer program for earthquake response analysis of horizontally layered sites. Report No. EERC 72-12, University of California, Berkeley, California.

Seed, H. B. and I. M. Idriss 1970. Shear moduli and damping factors for dynamic response analysis. Report No. EERC 70-10, University of California, Berkeley, California.